Fuel Processing Technology 199 (2020) 106293

Contents lists available at ScienceDirect

Fuel Processing Technology

journal homepage: www.elsevier.com/locate/fuproc

Research article

# Effect of Biodiesel impurities (K, Na, P) on non-catalytic and catalytic activities of Diesel soot in model DPF regeneration conditions

Hailong Zhang[a,b], Jishuang He[c], Shanshan Li[d], Eduard Emil Iojoiu[e], Maria Elena Galvez[a], Haifeng Xiong[b], Patrick Da Costa[a,*], Yaoqiang Chen[c,*]

[a] Sorbonne Université, Institut Jean Le Rond d'Alembert, CNRS, 2 place de la gare de Ceinture, 78210 Saint Cyr L'Ecole, France
[b] Department of Chemistry, College of Chemistry and Chemical Engineering, Xiamen University, Xiamen 361005, PR China
[c] College of Chemistry, Sichuan University, Chengdu 610064, PR China
[d] State Key Laboratory of Polymer Materials Engineering of China (Sichuan University), Polymer Research Institute of Sichuan University, Chengdu 610065, PR China
[e] Renault Trucks-Volvo Group Trucks Technology, Powertrain Engineering, 99 route de Lyon, 69806 Saint-Priest Cedex, France

ARTICLE INFO

*Keywords:*
Biodiesel soot
Biodiesel impurities
Potassium
Sodium
Phosphorus
Soot oxidation reactivity

ABSTRACT

The impact of Biodiesel impurities (Na, K and P) on the non-catalytic and catalytic reactivity of Diesel soot was evaluated under model DPF (Diesel Particulate Filter) regeneration conditions. Temperature-programmed oxidation (TPO) measurements confirmed that Na and K depositing into soot or on the surface of the catalyst enhanced the oxidative reactivity of soot under both $O_2$ and $NO_x + O_2$ and Na-doped samples showed better results. However, the presence of P inhibited the non-catalytic and catalytic reactivity. These findings can be mainly attributed to the changes in nanostructure and surface chemical properties of the doped samples, characterized by Raman, high-resolution transmission electron microscopy (HRTEM), X-ray photoelectron spectroscopy (XPS), $H_2$ temperature-programmed reduction ($H_2$-TPR) and NO temperature-programmed oxidation (NO-TPO). The result of this characterization evidenced that the presence of Na and K increased structural defects of soot and reduction ability of the catalyst. Moreover, Na-/K-doped catalysts presented higher oxidizing ability of NO into $NO_2$, whereas the opposite trend was observed for the P-containing catalysts. In addition, higher structural disorder of Na-doped soot and higher alkali metal content on the surface of Na-doped catalyst might lead to enhanced reactivity in comparison to K-doped soot and catalyst.

## 1. Introduction

Operation of diesel engines as lean burn engines can provide the user with good fuel economy due to their significant advantages in terms of high thermal efficiency and durability. Besides, high air/fuel ratios in their operation effectively reduce the emissions of gas phase hydrocarbons and carbon monoxide. However, severe emission problems related to particulate matter (PM), in particular, soot nanoparticles have caused serious environment pollution and human health influence [1–5]. Thus, many countries and regions have enacted more restrictive legislation such as Euro VI emission standard to limit PM emissions [6,7].

In order to comply with the restrictive emission standards, many researchers and vehicle manufacturers have been looking for an effective method to reduce PM emissions. Currently, Diesel Particulate Filter (DPF) with cordierite or silicon carbide (SiC) honeycomb structure has been widely applied in vehicles' exhaust aftertreatment system due to its high filtration efficiency [8]. Researchers also thought that the use of Biodiesel fuel as a renewable fuel can apparently decrease the emissions of carbon particulates and greenhouse gases (GHG) and thereby proposed to replace conventional Diesel fuel by Biodiesel [9,10]. Biodiesel fuel is a synthetic Diesel-like fuel and can be attained from natural sources such as vegetables and animal fats through transesterification of triglycerides [9,11]. In comparison with Diesel fuel, Biodiesel fuel has higher oxygen content, which would decrease the sooting tendency during fuel combustion and thereby soot deposit in the DPF [12–16]. Its combustion also results in the formation of oxygenated soot with more amorphous structure, thus improving its reactivity by oxidation [17–20].

Biodiesel fuel also contains some inorganic impurities such as alkali metals, phosphorus compounds, etc., these impurities may deposit all through the whole vehicle exhaust system during the combustion of large amount of Biodiesel [9,21,22]. Some inorganic elements may interact with the catalysts and soot particles, thereby influencing their

* Corresponding authors.
*E-mail addresses:* patrick.da_costa@sorbonne-universite.fr (P. Da Costa), chenyaoqiang@scu.edu.cn (Y. Chen).

https://doi.org/10.1016/j.fuproc.2019.106293
Received 18 September 2019; Received in revised form 18 November 2019; Accepted 18 November 2019
Available online 27 November 2019
0378-3820/ 

physicochemical properties and reactivity. It has been reported that in Diesel Oxidation Catalyst (DOC) and Selective Catalytic Reduction (SCR) systems, the presence of these impurities can lead to an important passivation of active sites resulting in the deactivation of the catalyst [22,23]. It was also found that in DPF, these impurities as ash exist on the monolith wall and also in the soot composition, thereby affecting the passive and active regeneration of DPF [22,24,25].

However, many studies have also confirmed that the presence of alkali metals in the catalysts has a positive impact on soot oxidation activity [26–33]. It was reported that the K-doped catalysts showed apparently improved catalytic activity during soot oxidation [27,28]. The researchers thought that the presence of potassium decreased the activation energy of soot oxidation reactions and thereby increased the reactivity. Gross et al. [29] studied the soot oxidation activity of ceria catalysts doped by $KNO_3$ and found a great enhancement of soot oxidation, they thought that high mobility of K improved the contact between soot particulates and catalyst and thus increased the availability of active sites in the catalyst. Aneggi et al. [30] studied the effect of Na, K, Rn and Cs alkali metals on soot oxidation activity of ceria, the result was found that all the elements showed an enhanced activity. Moreover, the intrinsic activity of some alkali metals was also studied through their impregnation on alumina support or directly on carbon black, it was found that Na, K and Cs have a catalytic role on carbon oxidation under air [31,32]. However, a few reports illustrate that the presence of phosphorus inhibits soot oxidation activity under $O_2$ [34–36]. Schobing et al. found that phosphorus has a beneficial effect on C-$NO_2$ reaction, particularly in presence of water [37]. Thus, the presence of these impurities in Biodiesel would affect the reactivity and catalytic activity of soot and so the regeneration of DPF. But the impact of inorganic elements or ash on non-catalytic and catalytic reactivities of real diesel soot in presence of $NO_x$ (NO and $NO_2$) in the feed gas is rarely reported in the literature.

During the passive regeneration of DPF, catalyst materials coated on DPF flow-wall substrates play an important role in improving soot oxidation activity. Many catalysts for soot oxidation have been extensively reported in the literature, such as noble metal catalysts [38,39], perovskite-type catalysts [40,41] and transition metal and ceria-based catalysts [42–46]. Among them, $MnO_x$-$CeO_2$ catalysts are relatively cheap and have excellent oxygen storage and redox ability and thus show high promotion on soot oxidation activity [44–46]. Moreover, $MnO_x$-$CeO_2$ mixed oxides are able to effectively oxidize NO into $NO_2$, thereby increasing C-$NO_2$ reaction activity, and also release a large amount of active oxygen species, as a result, improving soot oxidation by oxygen [46,47].

The aim of the present work is to study the impact of the presence of Biodiesel impurities on the DPF non-catalytic and catalytic regeneration under model DPF regeneration conditions. A real soot "B7", which generated from the combustion of common 7% Biodiesel-Diesel blends, was used in this work. The soot was doped by 0.5–2 wt% of inorganic elements (Na, K, P) to obtain the impurity-deposited soot samples. $MnO_x$-$CeO_2$ mixed oxides were used as the catalyst to evaluate the catalytic reactivity of soot. On the other side, in order to study the influence of Na, K and P elements on the catalytic performance of $MnO_x$-$CeO_2$ catalyst for soot oxidation, 1 wt% inorganic elements were doped into the catalyst. The novelty of this work is the use of real diesel soot obtained under cold drive cycles and the study on the impact of Biodiesel impurities on soot nanostructure and catalytic reactivity.

## 2. Experimental

### 2.1. Materials preparation

#### 2.1.1. Soot samples preparation

Real soot sample was prepared in an engine bench (Volvo Group Trucks Technology) through the combustion of fuels blend containing 7 vol% of Methyl Ester from rapeseed oil and 93 vol% of standard Euro VI fuel (EN 590). As shown in Fig. 1, the engine bench (8 L Diesel engine) was equipped with a Euro VI post-treatment system containing DOC and DPF. The system worked with a low loaded cycle operating at low temperatures, simulating very severe cold drive cycles. During this cycle, the average temperature of exhaust gases upstream the filter was around 160 °C. The produced soot particles were collected in DPF. The obtained soot sample was labeled as B7.

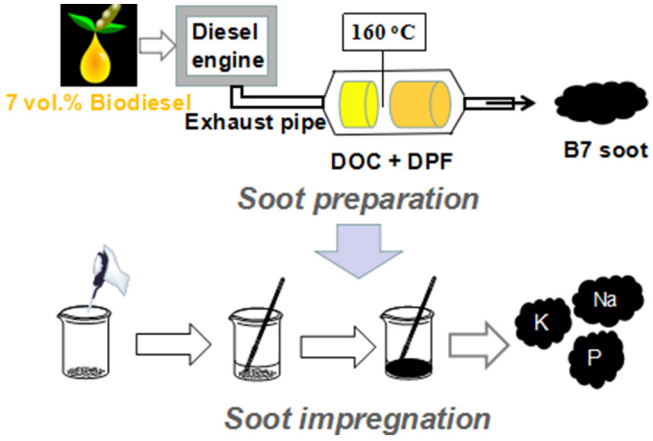


**Fig. 1.** Schematic diagram of soot preparation and impregnation.

Soot doping was performed through a saturated impregnation method (Fig. 1). First, the precursors $NaNO_3$, $KNO_3$ and $NH_4H_2PO_4$ were completely dissolved in a saturated porous volume of deionized water, respectively. Then 200 mg of soot powder B7 was taken into the solution, with continuous stirring. The final samples with 0.5 wt%, 1.0 wt% and 2.0 wt% inorganic elements were dried at 120 °C for a day and calcined in a muffle furnace at 350 °C for 2 h. The undoped soot was also calcined at the same temperature for 2 h and used as a reference, noted 350B7.

#### 2.1.2. Catalysts preparation

$MnO_x$-$CeO_2$ catalyst (Mn/Ce = 1/4 (mol/mol)) was prepared by a co-precipitation method. $Ce(NO_3)_3{\cdot}6H_2O$ (solid, 95% pure) and Mn $(NO_3)_2$ (liquid, 50 wt%) were used as the precursors. The details in materials preparation can be found elsewhere [20]. The obtained precipitates were calcined in static air at 500 °C for 3 h in a muffle furnace.

The obtained catalyst powder was separately impregnated 1.0 wt% inorganic elements by using an aqueous solution of $NaNO_3$, $KNO_3$ or $NH_4H_2PO_4$ using a saturated impregnation method. The doped samples were dried at 120 °C for a day and then calcined at 450 °C for 1 h. The final samples were noted X/Cat., X being the symbol of the inorganic elements. The undoped catalyst as a blank sample was also calcined under the same conditions and noted 450Cat.

### 2.2. Characterization techniques

Raman spectra of soot samples were characterized on a Raman system (Renishaw, London, England) with a YAG laser (532 nm). The output power of 0.9 mW was chosen in the scanning range of 800–2000 $cm^{-1}$.

X-ray photoelectron spectroscopy (XPS) measurement was conducted on an AXIS Ultra DLD spectrometer (Kratos, England) by using AlKα radiation as the excitation source (300 W). All binding energies (B.E.) were referenced to carbon C 1s line at 284.6 eV.

The textural characterization was conducted by $N_2$ adsorption at −196 °C in a BelSorb-Mini II (BEL-Japan) device. The BJH method was used for the calculation of the specific surface area and mean pore size.

The hydrogen temperature-programmed reduction ($H_2$-TPR) profiles of catalysts were performed by using a TP-5076 (Xianquan, Tianjing, China) apparatus equipped with a TCD (thermal conductivity

detector). The catalysts were pretreated at 450 °C for 45 min in He, then cooled down to 30 °C and heated until 700 °C in 5 vol% $H_2$/He at a heating rate of 10 °C/min.

The NO temperature-programmed oxidation (NO-TPO) experiments were carried out to evaluate the catalytic oxidation of NO into $NO_2$ on the catalysts. The mixture of 50 mg catalyst and 50 mg SiC powder was heated to 600 °C in tubular quartz reactor at the heating rate of 5 °C/min. The gas mixture of 400 ppm NO/9% $O_2$/$N_2$ was fed into the reactor at a flow rate of 250 ml/min. The concentration of the outlet gases (NO and $NO_2$) was detected by infrared-ray spectrometry (IR). The conversion ($Y$) of NO into $NO_2$ was calculated through the following formula:

$$Y = \frac{[NO_2]_{outlet}}{[NO_2]_{outlet} + [NO]_{outlet}} \times 100\%$$

### 2.3. Soot oxidation reactivity tests

The non-catalyzed and catalyzed oxidation activities of soot samples were measured by temperature program oxidation (TPO) method under different reaction gases: 9% $O_2$ + 5% $H_2O$ in Ar, 400 ppmv NO +9% $O_2$ + 5% $H_2O$ in Ar, 400 ppmv $NO_2$ + 9% $O_2$ + 5% $H_2O$ in Ar. Soot-TPOs were carried out in a U-shaped quartz reactor with a reaction bed of porous frit. Each sample was heated by a thermally isolated furnace at a heating rate of 10 °C. K-type thermocouple was used to monitor the temperature of the reaction bed. The total flow rate that passed through the reactor was controlled at 15 Nl/h (GHSV ≈ 100,000 $h^{-1}$) through mass flow meters (Brooks 5850S and Brooks Delta II). Concentrations of $CO_x$ (ppmv) in the outlet were recorded on Siemens Ultramat6 analyzer.

For the catalytic reactivity measurement, soot-catalyst mixture was prepared by loose contact method at a weight ratio of 1/10 (2.0 mg soot/20 mg catalyst). 2 mg soot sample was used for non-catalytic reactivity measurement. To minimize the influence of hot spots, the soot or mixture samples were diluted with 80 mg SiC pellets. In the obtained soot-TPO curves, $T_{5\%}$ and $T_{50\%}$ separately represent the temperatures at which 5% and 50% of soot conversion.

Based on the reaction C(soot) + $(1 + x) / 2O_2 \rightarrow xCO_2 + (1\text{-}x)CO$, the specific reaction rate ($V_{spec}$) was normalized to soot quality (2.0 mg) or catalyst mass (20 mg) and thus calculated by the following equation:

$$V_{spec} = \frac{(X_{CO} + X_{CO2}) \times D \times 10^{-3}}{3600 \times V_M \times m_{ini.}} \quad (a)$$

or

$$V_{spec} = \frac{(X_{CO} + X_{CO2}) \times D}{3600 \times V_M \times m_{cat.}} \quad (b)$$

where

$V_{spec}$: the specific reaction rate in (a) $mmol_{soot}/s/g_{ini.}$ or (b) $\mu mol_{soot}/s/g_{cat.}$,
$X_{CO}$ and $X_{CO2}$: molar fractions of CO and $CO_2$ in ppmv,
$D$: flow rate (15 Nl/h),
$V_M$: molar volume (22.4 L/mol),
$m_{ini.}$: mass of initial soot (0.002 g),
$m_{cat.}$: mass of catalyst (0.02 g).

## 3. Results and discussion

### 3.1. Soot oxidation under non-catalytic regeneration conditions

#### 3.1.1. Soot-TPOs in 9% $O_2$/Ar + 5% $H_2O$

Fig. 2 shows the TPO profiles of the B7 soot samples doped by K, Na and P with different concentrations under 9% $O_2$/Ar + 5% $H_2O$. It was found that the oxidative reactivity of B7 soot is apparently influenced by the presence of K, Na and P. As shown in Fig. 2a, the ignition of K/Na-doped samples takes place at lower temperatures compared to that of the undoped soot. The temperatures of the maximum soot oxidation rate visibly shift towards lower values after K and Na doping. With the doping amount of K and Na increasing from 0.5% to 2%, the oxidative reactivity of B7 trends to a better result. The promoting role of alkali metals on carbon oxidation by $O_2$ was also confirmed in the literature [23,31,32]. However, an opposite behavior of phosphorus can be seen in Fig. 2b, illustrating that the presence of P in soot inhibits the oxidative reactivity and the deposit of higher content of P leads to a worse result. The results are similar to previous studies [23,35,36]. The following Fig. 4 shows the temperatures at 5% or 50% conversion of different soot samples. It was found that under $O_2$, the reactivity follows the order: 1% Na/B7 > 1% K/B7 > 350B7 > 1% P/B7.

#### 3.1.2. Soot-TPOs in 400 ppm $NO_2$ + 9% $O_2$/Ar + 5% $H_2O$

Fig. 3 shows the TPO profiles of the doped soot samples under 400 ppm $NO_2$ + 9% $O_2$/Ar + 5% $H_2O$. The results seem to be similar with Fig. 2. It was also found that the presence of Na and K promotes the soot oxidation and 1% of element concentration exhibits higher promotion than the 0.5%. However, for 0.5% K/B7 sample, the ignition of soot occurs at higher temperature compared with that of undoped soot. In Fig. 4a, it is also observed that 1% K/B7 sample shows higher $T_{5\%}$ value than 350B7. It may be explained that partial $NO_2$ was stored in K/B7 in the form of nitrate and/or nitrite under 5% $H_2O$, thus decreasing C-$NO_2$ oxidation reaction rate at low temperatures. On the other hand, for the P-doped samples, it can be observed in Fig. 3 that 0.5% P/B7 sample seems to exhibit a slightly increased reactivity compared to 350B7. It was also noted in Fig. 4a that 1% P/B7 has a lower $T_{5\%}$ (358 °C) than 350B7 (372 °C). The results reveal that the presence of P also enhances the reactivity of soot under $NO_2$ + $O_2$ + $H_2O$, which was confirmed by Schobing et al. [23]. However, the peak temperature of 1% P/B7 visibly shifts to higher temperature relative to that of 350B7, their $T_{50\%}$ values also presenting the same trend (Fig. 4b). This indicates that P element inhibits high-temperature reactivity of soot. Fig. 4 illustrates the impact of different inorganic elements on soot oxidation reactivity in the presence of $NO_2$. $T_{5\%}$ and $T_{50\%}$ are as follows: 1% K/B7 > 350B7 > 1% P/B7 > 1% Na/B7 and 1% P/B7 > 350B7 > 1% K/B7 > 1% Na/B7, respectively.

In addition, it can be seen in Fig. 4a that the presence of $NO_2$ apparently decreases the $T_{5\%}$ values of soot samples, revealing the promoting role of $NO_2$ on soot oxidation at lower temperatures. While, as shown in Fig. 4b, the promotion of $NO_2$ becomes weak at higher temperatures ($T_{50\%}$), this is because thermal decomposition of $NO_2$ occurs and thereby decreases C-$NO_2$ or C-$NO_2$-$O_2$ reactions.

### 3.2. Soot oxidation under catalytic regeneration conditions

#### 3.2.1. Soot-TPOs in 9% $O_2$/Ar + 5% $H_2O$

The catalytic reactivity of the doped soot samples under 9% $O_2$/Ar + 5% $H_2O$ was evaluated through TPO and the results are presented in Fig. 5. The TPO profiles are very similar to those in absence of catalyst (Fig. 2). It was found in Fig. 5a that the presence of Na and K visibly enhances the catalytic reactivity of B7 soot in view of the TPO profiles shifting towards lower temperatures. While Fig. 5b shows that the presence of P inhibits soot catalytic oxidation. The reactivity of the soot samples doped by K, Na and P with different concentrations follows the order: 2% K/B7 > 1% K/B7 > 0.5% K/B7 > 350B7, 2% Na/B7 > 1% Na/B7 > 0.5% Na/B7 > 350B7 and 350B7 > 0.5% P/B7 > 1% P/B7 > 2% P/B7, respectively. The following Fig. 8 also illustrates the order of the reactivity ($T_{5\%}$ and $T_{50\%}$) of K/Na/P-doped samples is as follows: 1% Na/B7 > 1% K/B7 > 350B7 > 1% P. These results are similar with the previous non-catalytic reactivity under $O_2$.

In comparison with the previous C—$O_2$ reaction results in Fig. 4, the presence of catalyst visibly decreases the $T_{5\%}$ values of the undoped and

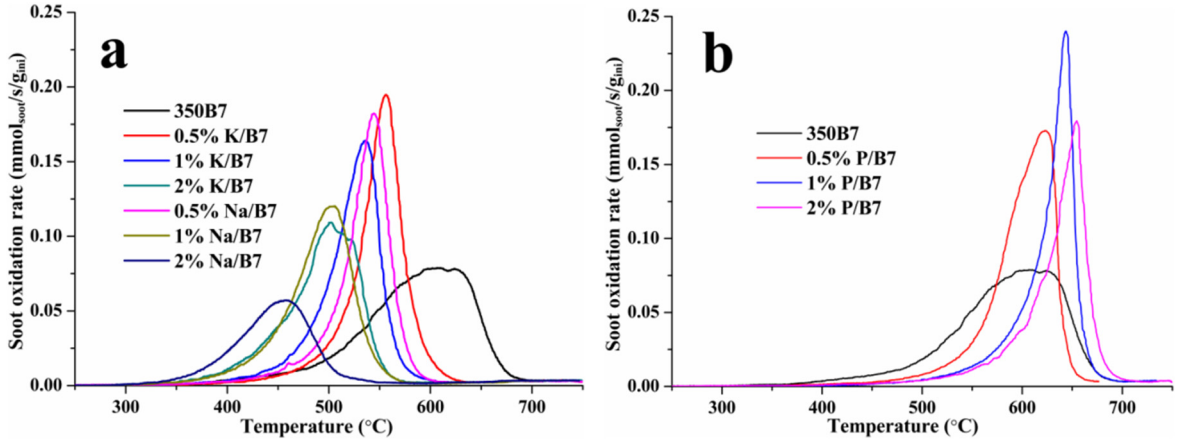


**Fig. 2.** TPO profiles of doped B7 soot under 9% $O_2$/Ar + 5% $H_2O$. 2 mg soot and 80 mg SiC powder were mixed, heating rate is 10 °C/min.

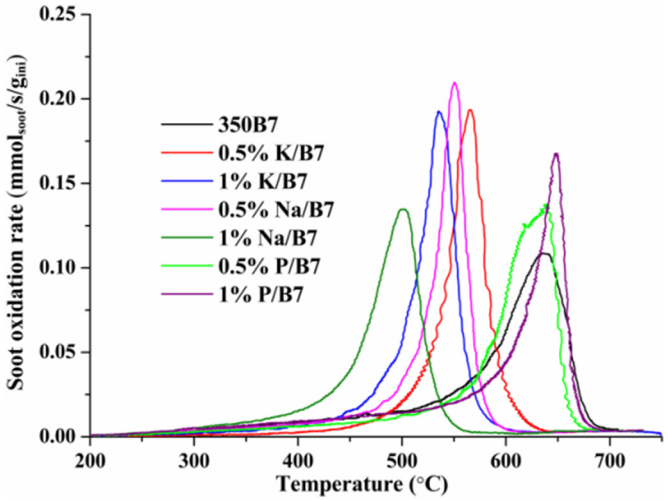


**Fig. 3.** TPO profiles of the doped soot samples under 400 ppm $NO_2$ + 9% $O_2$/Ar + 5% $H_2O$. 2 mg soot and 80 mg SiC powder were mixed, heating rate is 10 °C/min.

doped samples from 412–542 °C to 382–492 °C. While there is no an apparent difference in $T_{50\%}$ between with and without catalyst. This indicates that the presence of catalyst effectively promotes the ignition of soot.

### 3.2.2. *Soot-TPOs in 400 ppm NO +9% $O_2$/Ar + 5% $H_2O$*

Fig. 6 presents the TPO profiles of the doped soot samples with catalyst under 400 ppm NO +9% $O_2$/Ar + 5% $H_2O$. It was found that the soot oxidation reactions of all samples take place within a wider temperature window (200–700 °C) and the ignition of soot samples apparently shifts to lower temperatures compared to the results in $O_2$. Especially in Fig. 6a and b, it can be seen that all the TPO profiles move towards lower temperatures, which shows a strong promoting role of NO on soot catalytic oxidation, this has been confirmed in the previous studies [46–48]. However, in Fig. 6c, the presence of phosphorus does not make the peak temperature obviously shift towards lower temperatures after adding NO into reaction gas. This indicates that the presence of P weakens the promotion of NO on high-temperature activity.

Fig. 6a and b show that the presence of Na and K promotes the NO-assisted catalytic oxidation activity of soot except for 0.5% K-doped sample exhibiting a similar reactivity with undoped sample. Higher content of Na or K in soot leads to an increased reactivity. On the contrary, Fig. 6c reveals that the presence of P apparently inhibits the catalytic reactivity of soot. As presented in Fig. 5b, the deposit of more phosphorus in soot results in a larger decrease in the reactivity. In Fig. 8, it was found that $T_{5\%}$ and $T_{50\%}$ under NO + $O_2$ + $H_2O$ separately follow the order: 1% K/B7 > 1% Na/B7 > 1% P/B7 > 350B7 and 1% Na/B7 > 1% K/B7 > 350B7 > 1% P/B7. It is noted that during the ignition of soot, K-doped sample shows higher oxidative reactivity than Na-doped one and P-doped sample also exhibits an improved reactivity. This is different with the results in $O_2$. It illustrates that the impact of inorganic impurities on soot catalytic oxidation also depends on the composition of reaction gas.

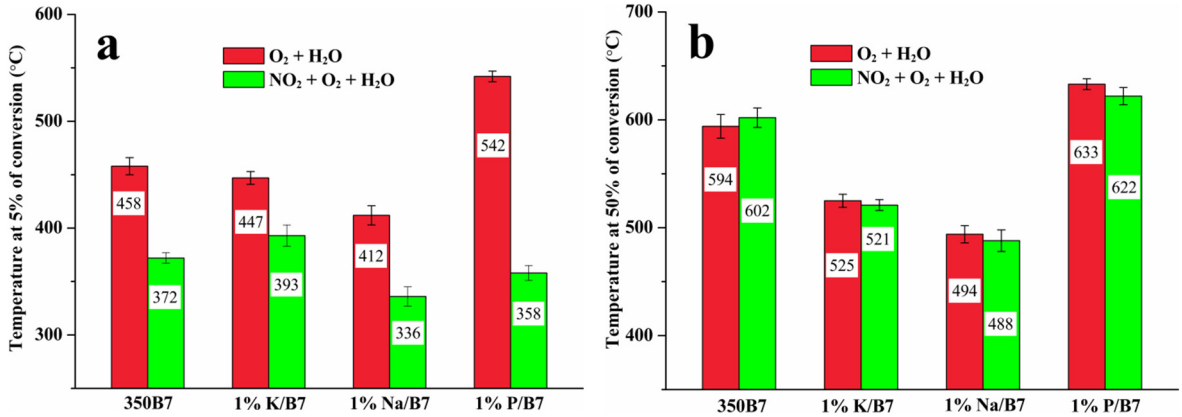


**Fig. 4.** Temperature for 5% of conversion ($T_{5\%}$) (a) and 50% of conversion ($T_{50\%}$) (b) of the 1 wt% doped soot samples.

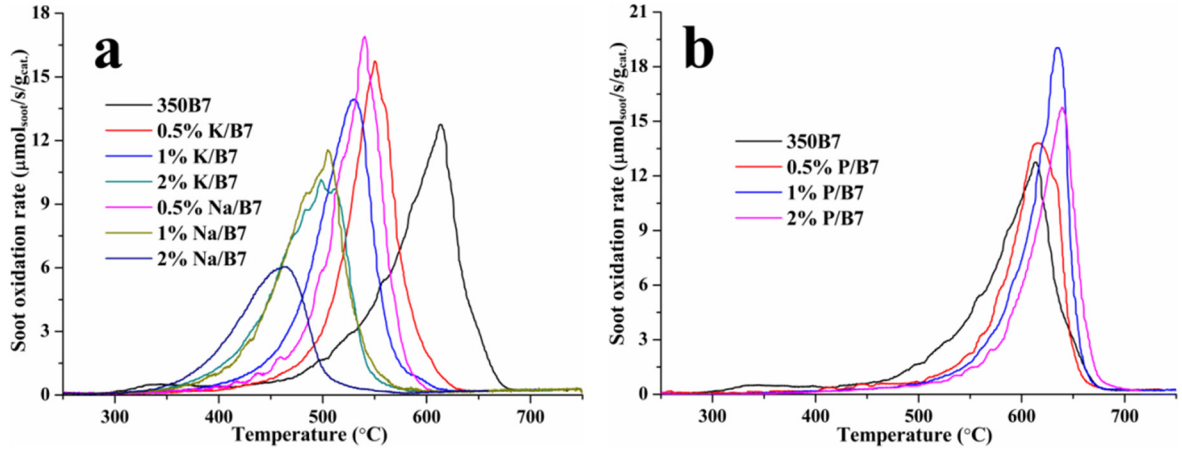


**Fig. 5.** TPO profiles of the doped soot samples with catalyst under 9% $O_2$/Ar + 5% $H_2O$. (a) K/Na-doped samples; (b) P-doped samples. 2 mg soot and 20 mg catalyst were mixed and then diluted by 80 mg SiC powder, heating rate is 10 °C/min.

*3.2.3. Soot-TPOs in 400 ppm $NO_2$ + 9% $O_2$/Ar + 5% $H_2O$*

The catalytic reactivity of the doped soot samples was also evaluated by TPO under 400 ppm $NO_2$ + 9% $O_2$/Ar + 5% $H_2O$ and the results are shown in Fig. 7 The TPO profiles seem to be similar with those under NO + $O_2$ + $H_2O$. The promotion of Na and K and the inhibition of P on soot oxidation are also observed here, but the promoting role of 0.5% K is not apparent. As shown in Fig. 8, $T_{5\%}$ and $T_{50\%}$ values of the doped samples under $NO_2$ + $O_2$ + $H_2O$ follow the order: 1% K/B7 ≈ 1% Na/B7 > 1% P/B7 > 350B7 and 1% Na/B7 > 1% K/B7 > 350B7 > 1% P/B7, respectively. The result also reveals the promoting role of P on soot ignition.

Fig. 8 presents $T_{5\%}$ and $T_{50\%}$ values of soot conversion profiles under different reaction gases. By comparison, the presence of $NO_x$ (NO and $NO_2$) visibly enhances the catalytic reactivity of soot. In the

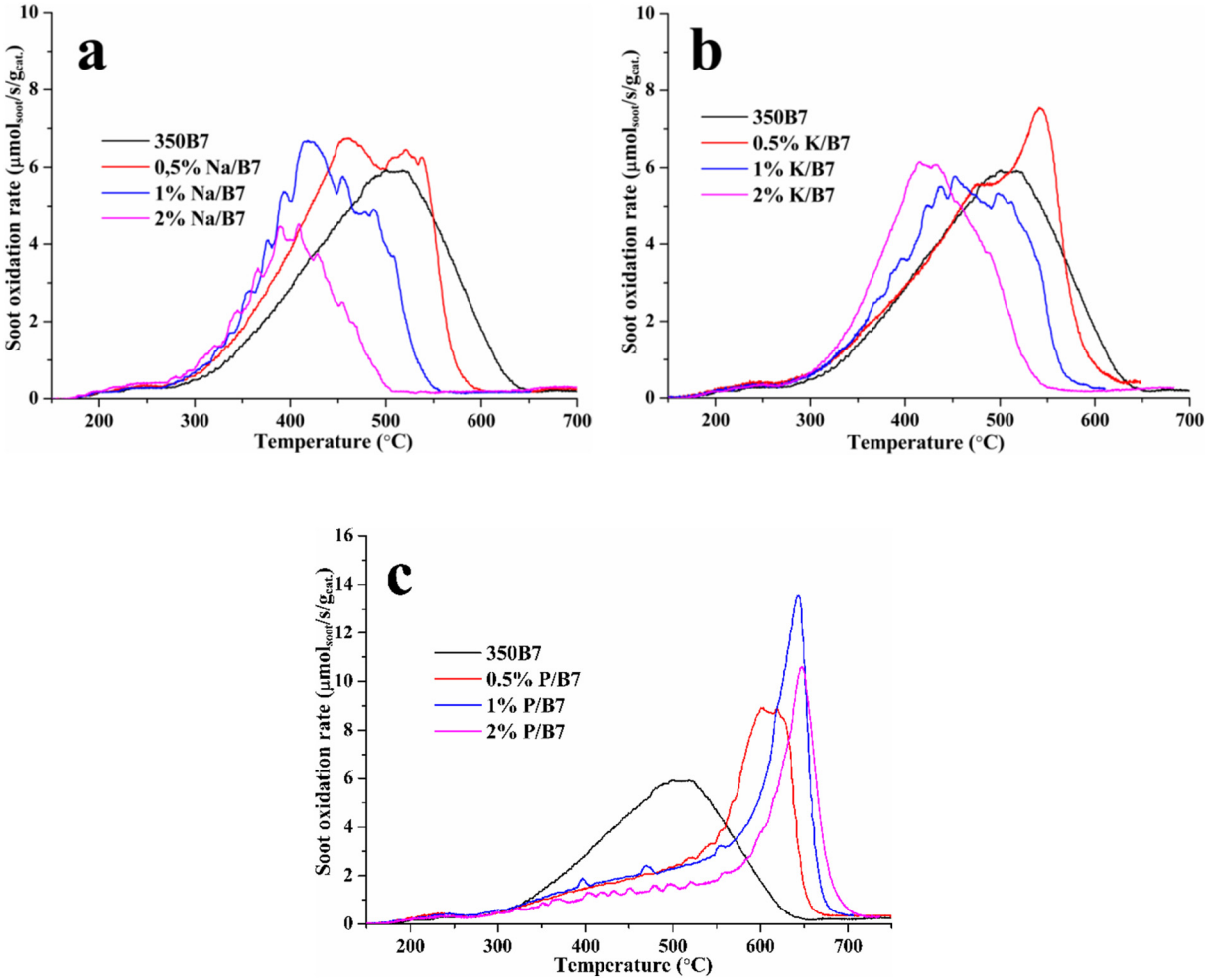


**Fig. 6.** TPO profiles of the doped soot samples with catalyst under 400 ppm NO + 9% $O_2$/Ar + 5% $H_2O$. (a) Na-doped samples; (b) K-doped samples; (c) P-doped samples. 2 mg soot and 20 mg catalyst were mixed and then diluted by 80 mg SiC powder, heating rate is 10 °C/min.

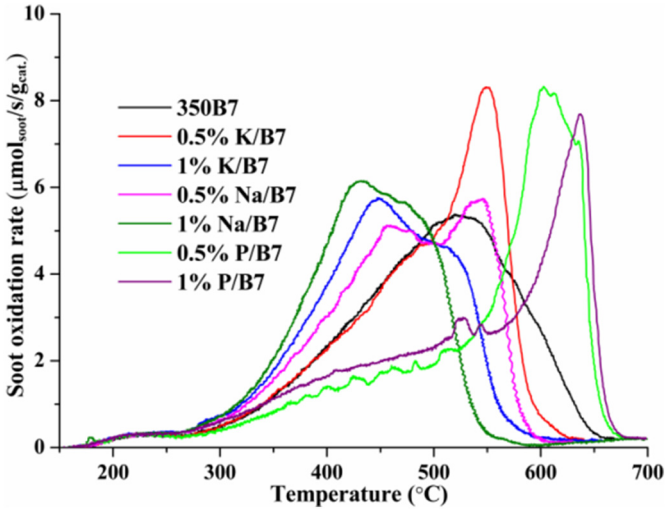


**Fig. 7.** TPO profiles of the doped soot samples with catalyst under 400 ppm $NO_2$ + 9% b.v. $O_2$/Ar + 5% $H_2O$. 2 mg soot and 20 mg catalyst were mixed and then diluted by 80 mg SiC powder, heating rate is 10 °C/min.

previous study [46], the authors compared the promoting role of NO and $NO_2$ during soot oxidation over Pt/$MnO_x$-$CeO_2$ catalyst and found that NO more highly promotes soot oxidation activity than $NO_2$. In Fig. 8, 1% K/B7 sample shows lower $T_{5\%}$ under NO, but the $T_{50\%}$ values under NO and $NO_2$ are very close. A similar $T_{5\%}$ under NO and $NO_2$ can be observed in 350B7 and 1% Na/B7 samples, while their $T_{50\%}$ values are lower under NO than that under $NO_2$. These may be attributed to higher promotion of NO. However, $T_{5\%}$ and $T_{50\%}$ of the P-doped sample all present a higher value under NO than that under $NO_2$, indicating higher promotion of $NO_2$.

### 3.3. Activity measurements of K, Na and P-doped catalysts

Under real exhaust conditions, the Biodiesel impurities such as Na, K and P presented in exhaust gas line can deposit on the surface of the catalysts coated on DPF substrates during DPF regeneration. These impurities may react with the catalysts and affect the catalytic reactivity of soot. Thus, in this work, 1 wt% Na, K and P were doped into Mn−Ce catalyst, respectively, to study their impact on the catalytic performance of the catalyst.

Fig. 9 shows the TPO profiles of the doped catalysts under different reaction gases. In the case of $O_2$ + $H_2O$, as shown in Fig. 9a, it was found that Na/Cat. and K/Cat. show apparently increased reactivity compared to 450Cat. and P/Cat. in the range of 350–550 °C and the former has higher reactivity than the latter. P/Cat. exhibits a similar reactivity with the undoped sample. The result confirms that the doping of K and Na into the catalyst can effectively promote the catalytic reactivity of C−$O_2$ reactions. Fig. 10 shows the $T_{50\%}$ of soot conversion of the doped catalysts under $O_2$ + $H_2O$, it also reveals the order of the reactivity is as follows: Na/Cat. (571 °C) > K/Cat. (594 °C) > P/Cat. (606 °C) ≈ 450Cat. (613 °C).

In adding NO and $NO_2$ into reaction gas, the TPO profiles shift towards lower temperatures and soot oxidation occurs in a wider temperature window (Fig. 9b and c). For the Na-doped catalyst, it shows higher catalytic reactivity and promoting role than K-doped catalyst in the presence of both NO and $NO_2$. The TPO profile under $NO_2$ + $O_2$ also moves to lower temperatures than that under NO + $O_2$ and thus exhibits lower $T_{50\%}$ value (Fig. 10). This indicates that the presence of $NO_2$ more highly increases the promoting role of Na on the catalytic activity. While the K-doped catalyst shows a similar catalytic activity under NO + $O_2$ and $NO_2$ + $O_2$ due to the close $T_{50\%}$ values (496 °C and 501 °C). Furthermore, K/Cat. shows similar reactivity with 450Cat. under $NO_2$ + $O_2$ because of their similar $T_{50\%}$ values, and an apparent promotion of K cannot be seen. Additionally, a visible inhibition of P on the catalytic reactivity can be observed in Fig. 9b and c. The presence of $NO_2$ also exhibits higher promoting role than NO for the P-doped catalyst in view of the lowered $T_{50\%}$ value (Fig. 10). Fig. 10 also illustrates the reactivity order of different catalysts: Na/Cat. > K/Cat. > 450 Cat. > P/Cat. under NO + $O_2$ and Na/Cat. > K/Cat. ≈ 450Cat. > P/Cat. under $NO_2$ + $O_2$, respectively.

### 3.4. Physicochemical characterization

#### 3.4.1. Soot characterization

*3.4.1.1. Raman analysis.* Fig. 11 as an example shows the Raman spectra of 350B7 sample, and the Raman results of other samples are not shown here because their Raman curves are similar (see the Supplementary materials, Fig. S1). It can be observed that there are two overlapping peaks, which appear at around 1350 $cm^{-1}$ (D peak) and 1580 $cm^{-1}$ (G peak), respectively [19,49,50]. The D peak, which includes D1, D2, D3 and D4 bands, is generally associated with the defective structure of carbon and the G peak is assigned to highly ordered graphitic structure. It was reported that D1 band at around 1350 $cm^{-1}$ is related to the disordered graphitic lattice and D3 band at around 1500 $cm^{-1}$ can provide some information about chemical structure of graphite-like and amorphous carbon, thus D1 FWHM (full width at half maximum) and relative intensity of D3 are considered to be important parameters to analyze carbon structure [50,51]. It was also reported that the FWHM of G and D bands and the relative intensity of D band ($I_D/I_G$) can be correlated to the degree of graphitization of carbonaceous materials [52–56]. The authors thought that higher order of carbon would be characterized by lower FWHM and $I_D/I_G$ values. Some researchers thought that the structural

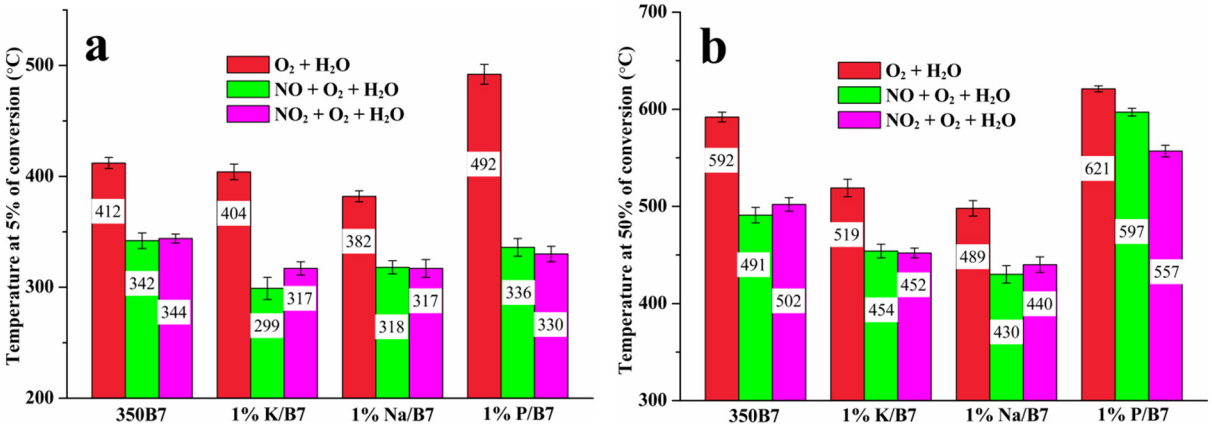


**Fig. 8.** Temperature for 5% of conversion ($T_{5\%}$) (a) and 50% of conversion ($T_{50\%}$) (b) of the 1 wt% doped soot samples.

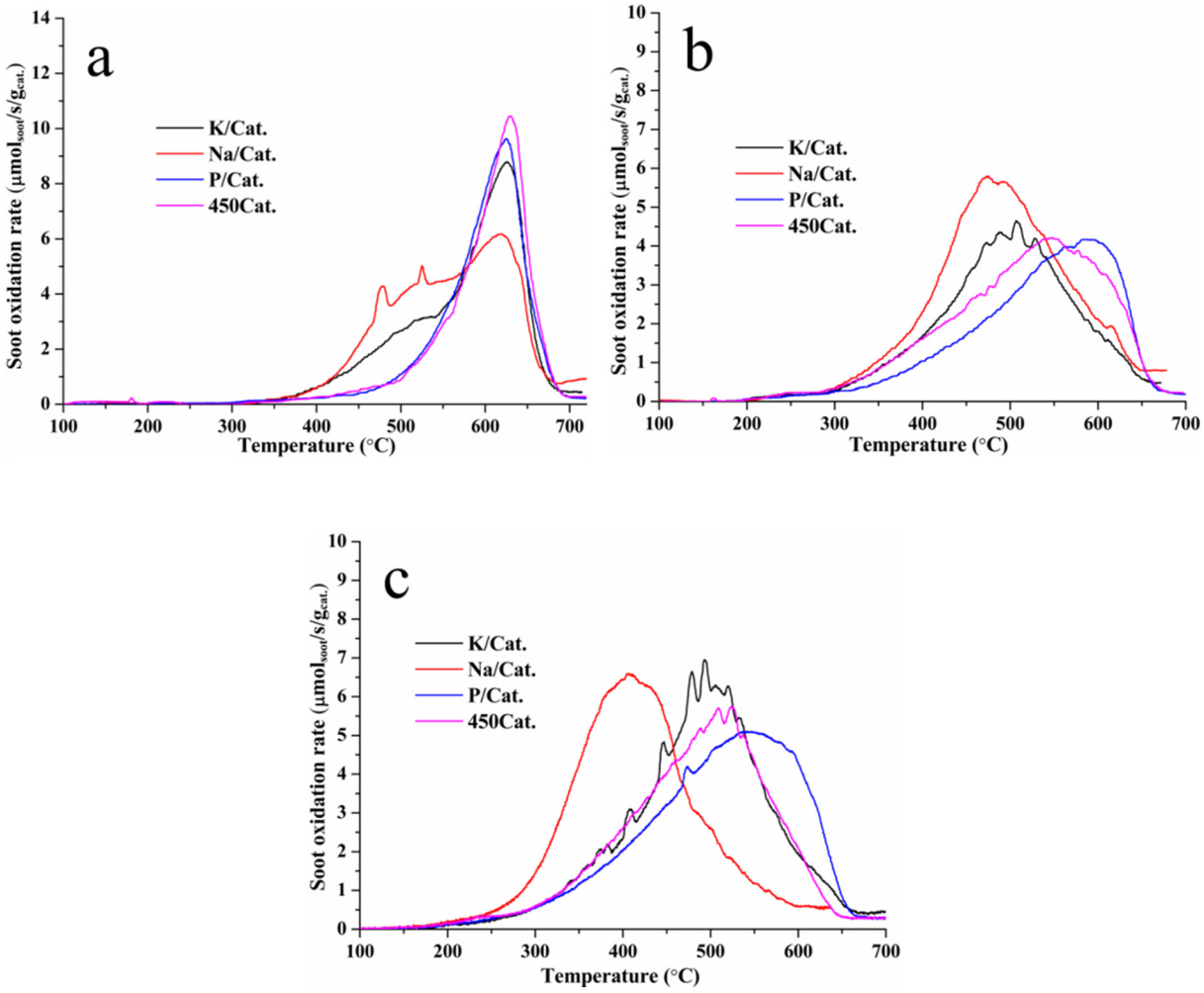


**Fig. 9.** TPO profiles of the doped catalysts under 9% $O_2$ + 5% $H_2O$ (a), 400 ppm NO + 9% $O_2$ + 5% $H_2O$ (b) and 400 ppm $NO_2$ + 9% $O_2$ + 5% $H_2O$ (c). The mass of 350B7 and catalyst was 2 mg and 20 mg, respectively, 80 mg SiC powder was used for dilution.

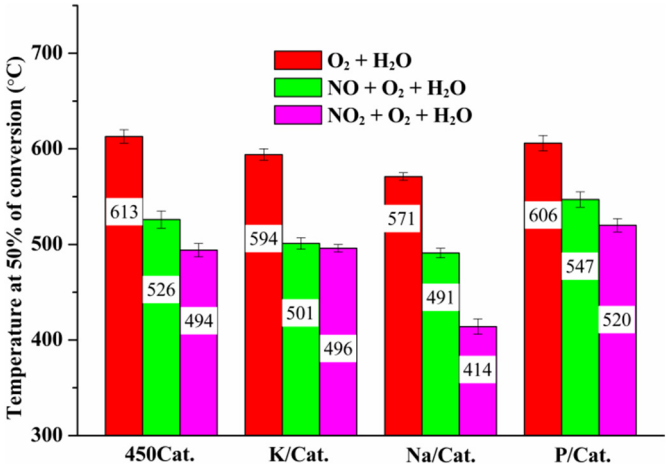


**Fig. 10.** Temperature for 50% of conversion ($T_{50\%}$) of the 1 wt% doped catalyst samples.

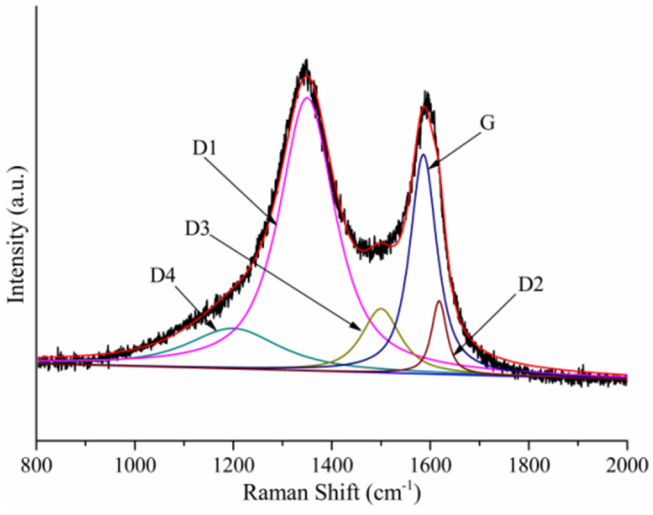


**Fig. 11.** Analysis of the Raman spectra and curve fits of 350B7 sample.

defects in graphene layers are also related to the ratios between D and G band areas ($A_D/A_G$) [51,57].

Table 1 shows the Raman results of different soot samples. In the case of K-doped samples, it can be noted that 0.5% K/B7 and 1% K/B7 samples show similar FWHM values of D1 and G bands as well as $I_{D1}/I_G$ and $I_{D3}/I_G$ compared to 350B7 sample. This illustrates that the degree of graphitization of the doped soot is not apparently affected by K. But it is also observed that the $A_{D3}/A_G$ of 1% K/B7 exhibits a visible increase from 0.42 ± 0.02 to 0.49 ± 0.04, which indicates that the addition of K into soot increases the structural defects. In case of Na-doped samples, they show similar D1 FWHM and $I_{D1}/I_G$ values compared to 350B7

**Table 1**
Raman results of soot samples.

| Sample | $FWHM_{D1}/cm^{-1}$ | $FWHM_G/cm^{-1}$ | $I_{D1}/I_G$ | $I_{D3}/I_G$ | $A_{D3}/A_G$ |
|---|---|---|---|---|---|
| 350B7 | 134 ± 14 | 65 ± 5 | 1.03 ± 0.11 | 0.91 ± 0.07 | 0.42 ± 0.02 |
| 0.5% K/B7 | 131 ± 13 | 64 ± 6 | 1.06 ± 0.13 | 0.89 ± 0.06 | 0.45 ± 0.04 |
| 1% K/B7 | 133 ± 13 | 67 ± 4 | 1.03 ± 0.13 | 0.92 ± 0.07 | 0.49 ± 0.04 |
| 0.5% Na/B7 | 131 ± 11 | 64 ± 7 | 1.04 ± 0.14 | 0.94 ± 0.08 | 0.57 ± 0.06 |
| 1% Na/B7 | 134 ± 14 | 72 ± 7 | 1.02 ± 0.11 | 0.95 ± 0.09 | 0.68 ± 0.07 |
| 0.5% P/B7 | 125 ± 10 | 67 ± 5 | 1.03 ± 0.15 | 0.93 ± 0.07 | 0.44 ± 0.01 |
| 1% P/B7 | 128 ± 15 | 67 ± 8 | 1.04 ± 0.12 | 0.91 ± 0.05 | 0.33 ± 0.03 |

sample, revealing a similar structure of the disordered graphitic lattice in carbon. It is also seen that 0.5% Na/B7 shows a very close G FWHM value while 1% Na/B7 reveals an obvious increase from 65 ± 5 to 72 ± 7 $cm^{-1}$ compared with 350 B7, this indicating that the doping of 1% Na into B7 soot decreases the degree of graphitization. Furthermore, the Na-doped samples show higher $I_{D3}/I_G$ and $A_{D3}/A_G$ values than 350 B7, this reveals that the introduction of Na apparently increases the number of defective sites and amorphous carbon. The 1% Na-doped sample displays more apparent result than 0.5% Na-doped sample. In comparison with K-doped samples, the addition of Na exhibits a higher promotion on increasing structural defects of carbon in view of higher $I_{D3}/I_G$ and $A_{D3}/A_G$ values.

For the P-doped samples, it can be noted that there is no an apparent change in G band FWHM, $I_{D1}/I_G$ and $I_{D3}/I_G$ values compared to 350B7 sample. However, their D1 band FWHM values decrease visibly, this may indicate an increased order in graphitic lattice. The 1% P-doped sample shows an apparent decrease in $A_{D3}/A_G$ from 0.42 ± 0.02 to 0.33 ± 0.03, which illustrates the decrease of structural defects in graphene layers. While $A_{D3}/A_G$ of 0.5% P-doped sample has no obvious change. The Raman results indicate that the introduction of P into soot causes a decreased trend of structural defects in carbonaceous materials.

In the previous reactivity results, K- and Na-doped soot samples show an improved reactivity under both non-catalytic and catalytic conditions. This could be attributed to their increased structural defects. The presence of Na in soot exhibits larger promotion on the reactivity than that of K, this is due to Na-doped soot presenting more structural defects than K-doped soot. However, P-doped samples show a decreased reactivity compared to 350B7, which would be related to the decreased trend of their structural defects.

*3.4.1.2. BET analysis*. The values of surface area ($S_{BET}$), micropore surface area, mesopore surface area, micropore volume ($V_{micro}$) and mesopore volume ($V_{meso}$) are listed in Table 2. Impregnation of B7 soot by K, Na and P significantly decreases the surface area and mesopore volume but increases micropore volume. This should be attributed to physical blocking of surface sites in pores. It can be noted that the addition of 0.5% K into soot leads to a sharp decrease in surface area but that of 1% K a slight decrease compared to 350B7 sample. It was reported that the impregnation of soot with alkali metals can result in a modification of the bulk carbonaceous structure through the insertion of the metals in the structure and thereby increase BET surface area and micropore volume [37]. This role of alkali metals might exist in the 1% K-doped soot sample, as a result, it shows much higher surface area than 0.5% K-doped soot sample. On the other side, for Na- and P-doped samples, their surface areas apparently decrease with the increase of the doping amount (from 0.5% to 1%).

**Table 2**
Specific surface area ($S_{BET}$), microporous pore volume ($V_{micro}$) and mesoporous pore volume ($V_{meso}$) of doped B7 soot samples.

| Sample | $S_{BET}$ ($m^2$/g) | Microporous $S_{BET}$ ($m^2$/g) | Mesoporous $S_{BET}$ ($m^2$/g) | $V_{micro}$ ($cm^3$/g) | $V_{meso}$ ($cm^3$/g) |
|---|---|---|---|---|---|
| 350B7 | 345 | 358 | 259 | $6.6 \times 10^{-3}$ | 1.63 |
| 0.5% K/B7 | 198 | 202 | 135 | $1.4 \times 10^{-2}$ | 0.34 |
| 1% K/B7 | 337 | 354 | 249 | $1.7 \times 10^{-2}$ | 0.64 |
| 0.5% Na/B7 | 286 | 323 | 188 | $1.7 \times 10^{-2}$ | 0.49 |
| 1% Na/B7 | 238 | 262 | 108 | $8.4 \times 10^{-2}$ | 0.17 |
| 0.5% P/B7 | 289 | 308 | 206 | $8.0 \times 10^{-2}$ | 0.54 |
| 1% P/B7 | 237 | 282 | 105 | $9.4 \times 10^{-2}$ | 0.16 |

However, the surface area and pore volume cannot be well correlated to the reactivity of the doped soot samples. For example, the introduction of Na and K greatly promotes the reactivity, but the doped samples present a decreased surface area. The result might illustrate that the reactivity of the doped soot samples do not depend on their surface area.

*3.4.1.3. HRTEM*. The morphology of different soot samples (including 350B7, 1% K/B7, 1% Na/B7 and 1% P/B7) was characterized through HRTEM, and the results are presented in Fig. 12. All samples exhibit highly ordered graphitic carbon layers and disordered amorphous structure. The crystalline layers in graphitic carbon exhibit strongly bent ribbons and long chainlike agglomerates. In the case of 350B7 sample, it can be observed that it shows visible and "tight" crystalline layers and high structural order. In the case of the doped soot samples, the Na- and K-doped samples exhibit less crystalline layers and more disordered carbon or amorphous carbon than 350B7 samples. But the morphology of K-doped sample shows more apparent crystalline layers than that of Na-doped sample. This result indicates that the presence of K and Na in soot increases the disordered structure and Na-doped sample shows a better result. For P-doped sample, due to the observation of a larger number of parallel stacked crystalline layers, it exhibits an increased order in carbon nanostructure compared to Na- and K-doped soot samples.

The previous Raman results reveal that the introduction of alkali metals (Na, K) into B7 soot increases the structural defects and that of P shows a decreased result, this point is also confirmed in these HRTEM images. The previous TPO results prove that the reactivities of soot samples follow Na/B7 > K/B7 > 350B7 > P/B7. The result is in good agreement with the structural and morphology features of soot.

*3.4.1.4. XPS analysis*. Figs. 13, 14 and 15 present the results of XP spectra of 350B7, 1% Na/B7 and 1% P/B7, respectively. It is difficult to analyze the XP spectra of 1% K/B7 (no shown) here due to the overlap of C1s and K2p XP spectra. It can be clearly observed in C1s XPS that the undoped and doped soot samples mainly consist of graphene, aliphatic carbon and molecular carbon (R-OH, C-O-C, -COOH, -C(O)-O-C, -C=O, etc.) [34,35]. The O1s XPS reveal that the detected oxygen mainly originates from carbon-oxygen complexes (CO). The XP spectrum of the S2p (BE = 168.63 eV and 166.30 eV) [58,59], which is not shown here due to lower sulfur content, also illustrates the presence of sulfur in B7 soot. In 1% Na/B7 sample (Fig. 14), the O1s XP spectrum detected the presence of S in the form of $SO_x$ at 531.55 eV, which may be attributed to the formation of $Na_2SO_x$ (x = 3 or 4) [37]. The XP spectrum of Na1s shows that Na was only detected in the form of sulfate/sulfonate at 1071.36 eV [37]. In the case of 1% P/B7 (Fig. 15), Phosphorous was detected in the form of phosphate at

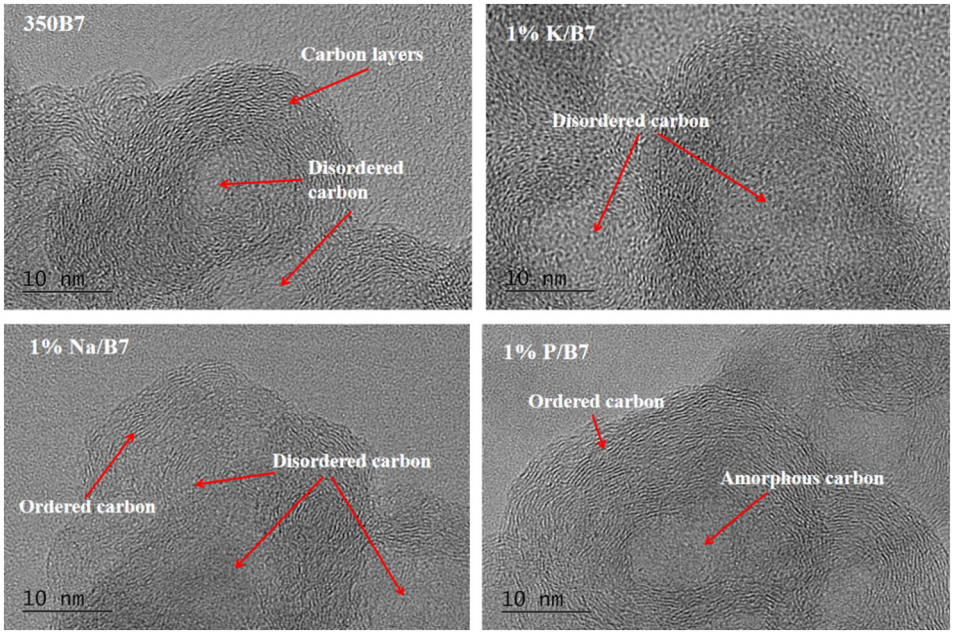


**Fig. 12.** HRTEM images of different soot samples.

133.71 eV [34,35]. Thus, the single (O—P) and double bindings (O = P) were also detected in the O1s XP spectra (O-P: 531.45 eV; O = P: 532.85 eV) [34].

Table 3 lists the elemental composition of the soot samples in wt% determined by XP Spectroscopy. It can be seen that the doped samples (1% Na/B7 and 1% P/B7) exhibit higher oxygen content than 350B7 sample, this may be due to the formation of sulfate and phosphate species. But 1% Na/B7 sample shows the highest oxygen content in (CO) form, which may be ascribed to the formation of more surface (CO) species. Higher sulfur content of 1% Na/B7 soot is likely attributed to the formation of $Na_2SO_x$ decreasing the loss of sulfur during calcination step. Table 3 also illustrates that the content of Na in Na-doped sample (1.2%) is higher than the theoretical content (1%) and that of P in P-doped sample (0.5%) is much lower than the theoretical one (1%). The lower content of P may result from partial P entering into the bulk structure of carbon and forming C-O-$PO_3$ or $(CO)_3$-P species [34–37].

The previous TPO results reveal that Na-doped soot sample shows higher non-catalytic and catalytic reactivity under both $O_2$ and $NO_x + O_2$ than 350B7 and P-doped soot sample. The XPS results confirm that 1% Na/B7 shows higher oxygen content (14.3%), especially that in (CO) form (13.4%), than 350B7 and 1% P/B7. This might be one of factors that promote soot oxidation reactivity. Besides, the P-doped sample shows a similar oxygen content with 350B7 sample, however, this cannot explain an obvious inhibition of P on soot oxidation reactivity. This is because the oxygen content on the carbon surface is not the only one factor that determines the reactivity of soot. The previous Raman and HRTEM results reveal that 1% P/B7 exhibits an increase in structural order, which might be a key factor that leads to the decrease of the reactivity.

On the other side, other factors may also determine the reactivity of soot. For example, the presence of K or Na in soot could play a role of catalyst to decrease the activation energy of soot oxidation, thus improving the reactivity [28,31,32]. Moreover, K also promotes the contact between catalyst and soot due to its high mobility and thereby the catalytic reactivity [29].

### 3.4.2. Catalyst characterization

In real Diesel exhaust system, the combustion of Biodiesel soot during DPF regeneration would lead to Biodiesel impurities (Na, K, P) depositing the surface of the catalyst that was coated on the DPF substrate. To study the impact of these impurities on chemical performances of the catalyst, $H_2$-TPR, XPS and NO-TPO experiments were performed in this work.

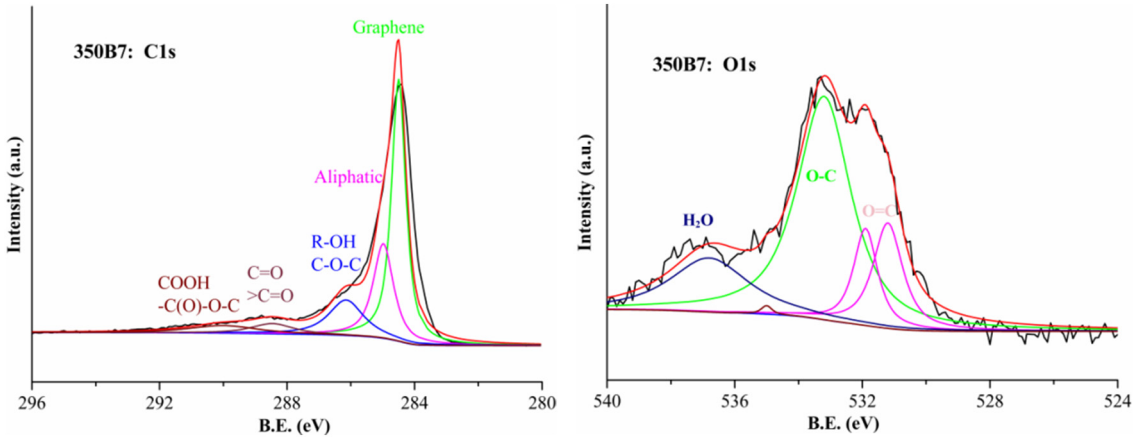


**Fig. 13.** XP spectra of C1s, O1s of 350B7 soot sample.

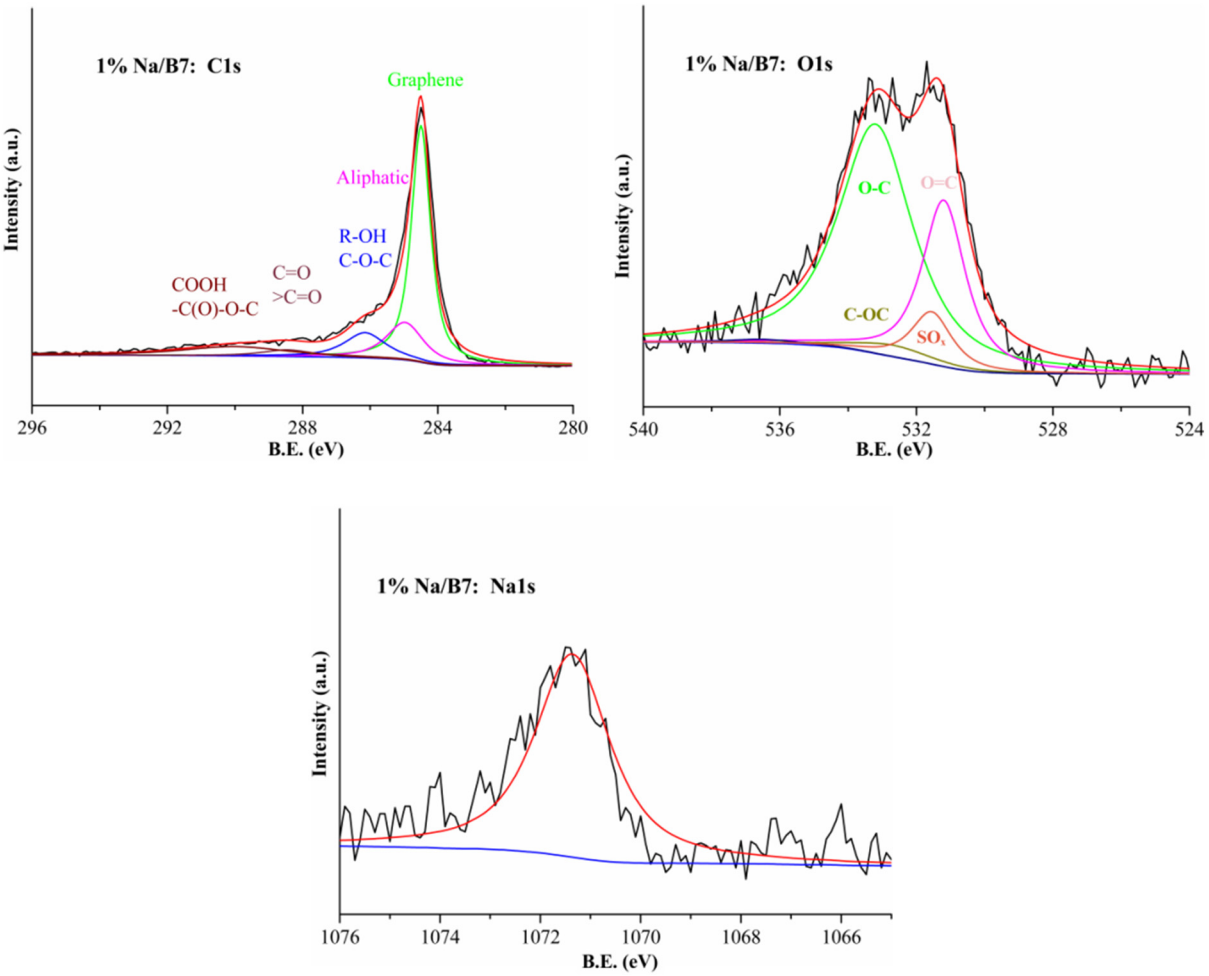


**Fig. 14.** XP spectra of C1s, O1s, Na1s of 1% Na/B7 soot sample.

*3.4.2.1. $H_2$-TPR*. The $H_2$-TPR profiles of the undoped and doped catalysts are shown in Fig. 16. It can be observed that the undoped $MnO_x$-$CeO_2$ catalyst shows a wide overlapped peak from 150 to 550 °C. This overlapped peak includes three reduction steps, which might separately be the reduction of "isolated" $Mn^{4+}$ ions, $Mn^{\delta+}$ species in Mn−Ce solid solution and synergistic Mn/Ce species [60,61]. In the case of the doped catalysts, the K- and Na-doped samples show a sharp reduction peak at 281 and 301 °C, respectively. This result confirms that alkali metals increase the reduction rate of Mn−Ce mixed oxides. Besides, the $H_2$ consumption at temperatures from 480 to 650 °C may be attributed to the reduction of $NO_3^-$ ions, which were not fully decomposed during calcination at 450 °C, by $H_2$ into $N_2$ [62]. However, the reduction steps of the P-doped sample shift towards higher temperatures compared to the undoped sample, which indicates that the presence of P inhibits the reduction of the catalyst.

The previous TPO results show that alkali metals effectively enhance the soot oxidative activity of the catalyst, this being attributed to K and Na improving the reduction ability of the catalyst. Moreover, it is noted that in Fig. 16, K-doped sample exhibits slightly higher reduction ability than Na-doped sample, but it presents lower soot oxidation reactivity. This illustrates that the reduction ability is one of the factors that affect the catalytic reactivity. Besides, the decreased reactivity of P-doped catalyst should be correlated to the inhibition of P on the reduction ability.

*3.4.2.2. XPS analysis*. Table 4 presents the relative content of different elements on the surface of the undoped and doped catalysts based on XPS spectra (see the Supplementary materials, Fig. S2). It is observed that in comparison with the undoped catalyst, the doped catalysts present a decreased content of Mn and Ce elements. The introduction of Biodiesel impurities into the catalyst also influences the chemical states of Mn and Ce. For example, the $Mn^{4+}$ concentration of the catalyst apparently decreases after adding Na, K and P, Na-doped catalyst shows an increased $Mn^{2+}$ or $Ce^{3+}$ concentration but K-/P-doped catalysts present a decreased value. Besides, the content of surface oxygen species in the doped catalysts increases from 13% to 17.0–24.8%. It was reported that the soot oxidation reactivity of Mn−Ce catalysts is related to the amount of surface oxygen species, their higher content would lead to a higher reactivity [61]. Thus, the previous TPO results show that Na- and K-doped catalysts present higher reactivity than the undoped catalyst. While P-doped sample with higher content (24.8%) of surface oxygen species exhibits an inhibition in the reactivity, this may be because the presence of P decreases the reduction ability of the catalyst ($H_2$-TPR). Its high surface oxygen content might be ascribed to the formation of phosphorus oxides. In addition, in Table 4, it can be noticed that Na-doped catalyst has higher deposit of alkali metal (8.97%) than K-doped catalyst (2.94%). According to the literature [28,31,32], the presence of K or Na could catalyze the oxidation of soot and thereby improve the reactivity. Therefore, higher deposit of Na on the surface of the catalyst would more apparently increase the catalytic reactivity of soot, this may be one of the factors that result in higher reactivity of Na-doped catalyst than K-doped catalyst.

*3.4.2.3. NO-TPO*. It is well known that $NO_2$ has higher ability to oxidize soot particles than $O_2$ at low temperatures [44–47]. Thus, the conversion of NO into $NO_2$ is important for the catalytic reactivity of

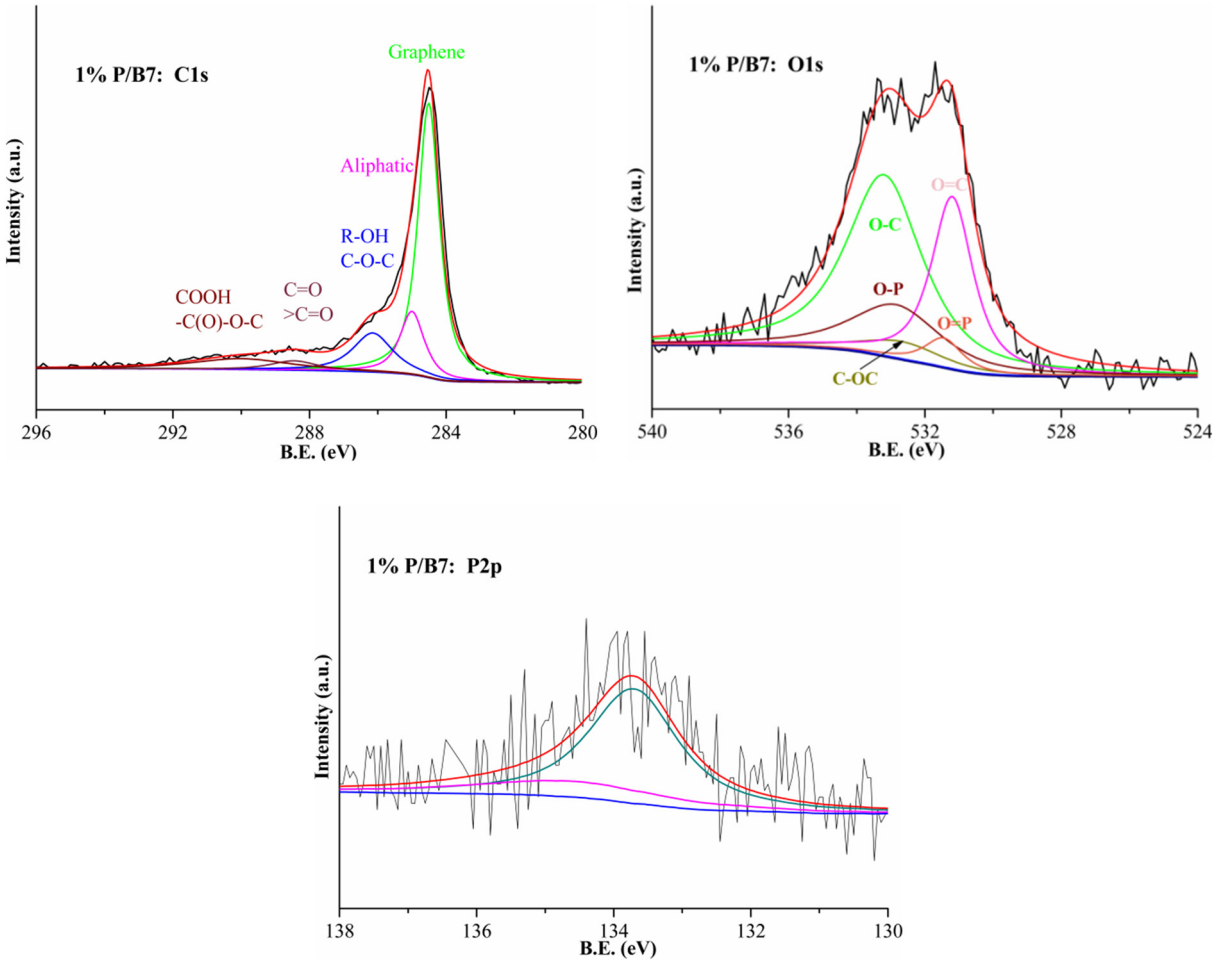


**Fig. 15.** XP spectra of C1s, O1s, P2p of 1% P/B7 soot sample.

**Table 3**
Elemental composition of the soot samples in wt% determined by XP Spectroscopy.

| Sample | C | O | $O_{(CO)}$ | S | Na | P |
|---|---|---|---|---|---|---|
| 350B7 | 86.3 | 13.6 | 10.9 | 0.2 | / | / |
| 1% Na/B7 | 84.1 | 14.3 | 13.4 | 0.3 | 1.2 | / |
| 1% P/B7 | 85.2 | 14.1 | 10.6 | 0.2 | / | 0.5 |

soot in the presence of NO. In this work, NO-TPO experiments were tested to evaluate the oxidizing ability of NO into $NO_2$ in the catalysts. As shown in Fig. 17, in comparison with the undoped catalyst, the doped catalysts show lower production of $NO_2$. But it can be noted that Na- and K-doped catalysts exhibit similar NO-TPO profiles and their peak temperatures shift towards lower values, and the NO-TPO profile of P-doped sample, on the contrary, shift to higher temperatures. This result indicates that Na and K promote the oxidizing ability of NO and P inhibits that. The previous $H_2$-TPR results also confirm an obvious promotion of K and Na and an inhibition of P on reduction ability, this may result in the results above.

The previous TPO results show that K-/Na-doped catalysts exhibit higher reactivity of soot ($T_{50\%}$ = 491–501 °C) than the undoped catalyst ($T_{50\%}$ = 526 °C) in the presence of NO, which might be related to their higher oxidizing ability of NO into $NO_2$. Moreover, in the previous work [46,63], the authors proposed that the soot oxidation reaction is related to the C + $NO_2$ + $O_2$/O* (active oxygen) cooperative reaction. The XPS and $H_2$-TPR results show that Na/K alkali metals increase the content of surface oxygen species and reduction ability of the catalyst,

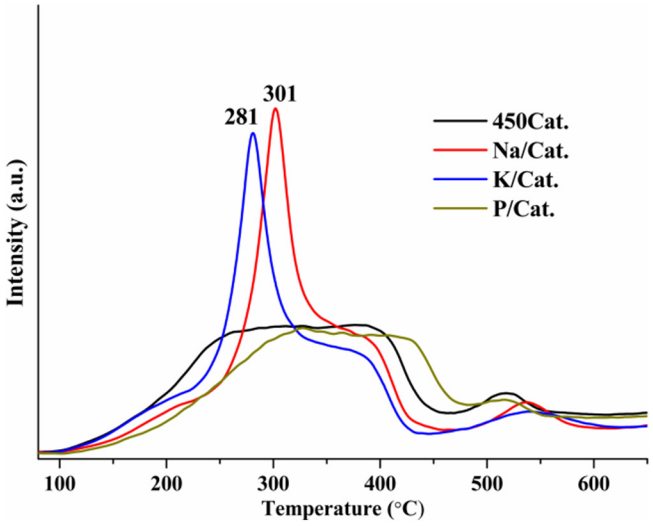


**Fig. 16.** $H_2$-TPR results of undoped and doped catalysts.

this might indicate Na and K enhance the release rate of active oxygen (O*), thereby improving the cooperative reaction rate. Thus, the decreased reactivity of P-doped catalyst in the presence of NO might be attributed to the decrease of reduction ability and NO oxidizing ability into $NO_2$.

**Table 4**
XPS results of undoped and doped catalysts.

| Catalyst | Element (at.%) | | | | | | $Ce^{3+}$/Ce (at.%) | Mn (at.%) | | | O (at.%) | |
|---|---|---|---|---|---|---|---|---|---|---|---|---|
| | Ce | Mn | O | Na | K | P | | $Mn^{4+}$ | $Mn^{3+}$ | $Mn^{2+}$ | $O_{latt}$ | $O_{sur}$ |
| Cat. | 29.7 | 7.73 | 62.5 | / | / | / | 11.8 | 2.14 | 1.65 | 1.37 | 49.5 | 13.0 |
| Na/Cat. | 27.7 | 5.03 | 58.3 | 8.97 | / | / | 13.0 | 0.33 | 1.04 | 1.70 | 40.1 | 18.2 |
| K/Cat. | 28.5 | 4.61 | 63.9 | / | 2.94 | / | 10.2 | 0.28 | 1.68 | 0.96 | 46.9 | 17.0 |
| P/Cat. | 27.0 | 5.65 | 63.8 | / | / | 3.53 | 11.2 | 0.37 | 1.97 | 0.81 | 39.0 | 24.8 |

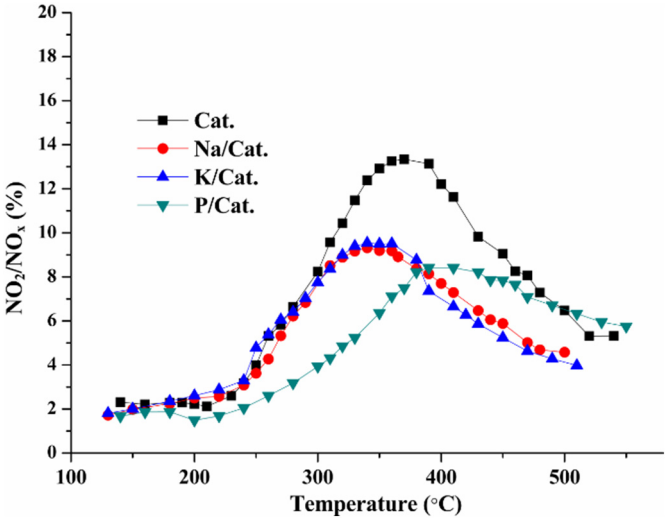


**Fig. 17.** NO-TPO curves of undoped and doped catalysts. Reaction conditions: catalyst mass = 50 mg, SiC powder mass = 50 mg, reaction gas is 400 ppm NO + 9% $O_2$ + $N_2$, heating rate is 5 °C/min.

## 4. Conclusion

A real Biodiesel-Diesel soot and $MnO_x$-$CeO_2$ catalyst were impregnated by Na, K and P through a saturated impregnation method. The non-catalytic and catalytic reactivity of soot were evaluated under model DPF regeneration conditions. TPO results confirm that the introduction of Na and K enhanced the non-catalytic and catalytic reactivity of soot under both $O_2$ and $NO_x$ + $O_2$ and Na-doped sample shows better results. The presence of P in soot or catalyst inhibits the reactivity in view of the increased $T_{50\%}$ value. The characterizations reveal that the soot doped with Na and K exhibits an increase of the structural defects and a decrease of the ordered structure. Moreover, Na-/K-doped catalysts show an increase in the reduction ability and the NO oxidizing ability into $NO_2$. Opposite results were found on P-doped samples. Higher reactivity of Na-doped soot is mainly ascribed to its higher structural disorder compared with K-doped soot.

## CRediT authorship contribution statement

**Hailong Zhang:** Investigation, Methodology, Writing - original draft, Writing - review & editing. **Jishuang He:** Investigation, Writing - original draft. **Shanshan Li:** Investigation, Writing - original draft. **Eduard Emil Iojoiu:** Resources, Validation, Writing - original draft, Writing - review & editing. **Maria Elena Galvez:** Investigation, Writing - original draft. **Haifeng Xiong:** Methodology, Writing - review & editing. **Patrick Da Costa:** Writing - original draft, Writing - review & editing, Funding acquisition, Supervision. **Yaoqiang Chen:** Writing - original draft, Writing - review & editing, Funding acquisition, Supervision.

## Declaration of competing interest

The authors declare that they have no known competing financial interests or personal relationships that could have appeared to influence the work reported in this paper.

## Acknowledgements

The authors would like to thank: (a) Volvo Group Trucks Technology-Renault Trucks for the real Biodiesel-Diesel soot, (b) Yaoqiang's group for providing the catalyst materials, (c) Institut Jean Le Rond d'Alembert, Sorbonne Université and College of Chemistry, Sichuan University for all the facilities for this work.

## Appendix A. Supplementary data

Supplementary data to this article can be found online at https://doi.org/10.1016/j.fuproc.2019.106293.

## References

[1] M.V. Twigg, Progress and future challenges in controlling automotive exhaust gas emissions, Appl. Catal. B 70 (2007) 2–15.
[2] P. Fornasiero, T. Montini, M. Graziani, S. Zilio, M. Succi, Development of functionalized Fe-Al-Cr alloy fibers as innovative catalytic oxidation devices, Catal. Today 137 (2008) 475–482.
[3] M.V. Twigg, Catalytic control of emissions from cars, Catal. Today 163 (2012) 33–41.
[4] D.C. Quiros, S. Yoon, H.A. Dwyer, J.F. Collins, Y.F. Zhu, T. Huai, Measuring particulate matter emissions during parked active diesel particulate filter regeneration of heavy-duty diesel trucks, J. Aerosol Sci. 73 (2014) 48–62.
[5] A. Valavanidis, K. Fiotakis, T. Vlahogianni, E.B. Bakeas, S. Triantafillaki, V. Paraskevopoulou, et al., Characterization of atmospheric particulates, particle-bound transition metals and polycyclic aromatic hydrocarbons of urban air in the centre of Athens (Greece), Chemosphere 65 (2006) 760–768.
[6] Direction générale des Infrastructures, des Transports et de la Mer-Des véhicules aux normes pour réduire la pollution de l'air, (2011).
[7] M.A. Mokhri, N.R. Abdullah, S.A. Abdullah, S. Kasalong, R. Mamat, Soot filtration recent simulation analysis in diesel particulate filter (DPF), Procedia Eng 41 (2012) 1750–1755.
[8] İ.A. Reşitoğlu, K. Altinişik, A. Keskin, The pollutant emissions from diesel-engine vehicles and exhaust aftertreatment systems, Clean Techn. Environ. Policy 17 (2015) 15–27.
[9] A.K. Agarwal, T. Gupta, P.C. Shukla, A. Dhar, Particulate emissions from biodiesel fuelled CI engines, Energ. Convers. Manage. 94 (2015) 311–330.
[10] J. Xue, T.E. Grift, A.C. Hansen, Effect of biodiesel on engine performances and emissions, Renew. Sust. Energ. Rev. 15 (2011) 1098–1116.
[11] U. Schuchardt, R. Sercheli, R.M. Vargas, Transesterification of vegetable oils: a review, J. Brazil. Chem. Soc. 9 (1998) 199–210.
[12] R.L. Schalla, G.E. McDonald, Variation in smoking tendency, J. Ind. Eng. Chem. 45 (1953) 1497–1500.
[13] R. Lemaire, D. Lapalme, P. Seers, Analysis of the sooting propensity of C-4 and C-5 oxygenates: comparison of sooting indexes issued from laser-based experiments and group additivity approaches, Combust. Flame 162 (2015) 3140–3155.
[14] A.M. Dmitriev, D.A. Knyazkov, T.A. Bolshova, A.G. Shmakov, O.P. Korobeinichev, The effect of methyl pentanoate addition on the structure of premixed fuel-rich *n*-heptane/toluene flame at atmospheric pressure, Combust. Flame 162 (2015) 1964–1975.
[15] H.J. Seong, A.L. Boehman, Studies of soot oxidative reactivity using a diffusion flame burner, Combust, Flame 159 (2012) 1864–1875.
[16] C.S. McEnally, L.D. Pfefferle, Sooting tendencies of oxygenated hydrocarbons in laboratory-scale flames, Environ. Sci. Technol. 45 (2011) 2498–2503.
[17] J. Song, M. Alam, A.L. Boehman, U. Kim, Examination of the oxidation behavior of biodiesel soot, Combust. Flame 146 (2006) 589–604.
[18] N. Lamharess, C.N. Millet, L. Starck, E. Jeudy, J. Lavy, P.D. Costa, Catalysed diesel

particulate filter: study of the reactivity of soot arising from biodiesel combustion, Catal. Today 176 (2011) 219–224.
[19] J. Abboud, J. Schobing, G. Legros, J. Bonnety, V. Tschamber, A. Brillard, et al., Impacts of oxygenated compounds concentration on sooting propensities and soot oxidative reactivity: application to Diesel and Biodiesel surrogates, Fuel 193 (2017) 241–253.
[20] H.L. Zhang, O. Pereira, G. Legros, E.E. Iojoiu, M.E. Galvez, Y.Q. Chen, P.D. Costa, Structure-reactivity study of model and Biodiesel soot in model DPF regeneration conditions, Fuel 239 (2019) 373–386.
[21] P.C. Shukla, T. Gupta, N.K. Labhsetwar, A.K. Agarwal, Trace metals and ions in particulates emitted by biodiesel fuelled engine, Fuel 188 (2017) 603–609.
[22] D.W. Brookshear, K. Nguyen, T.J. Toops, B.G. Bunting, W.F. Rohr, J. Howe, Investigation of the effects of biodiesel-based Na on emissions control components, Catal. Today 184 (2012) 205–218.
[23] J. Schobing, V. Tschamber, J.F. Brilhac, A. Auclaire, R. Vonarb, Investigation of the impact of calcium, zinc and phosphorus on deNO$_x$, Top. Catal. 59 (2016) 1013–1019.
[24] A. Liati, A. Spiteri, D.P. Eggenschwiler, N. Vogel-Schäuble, Microscopic investigation of soot and ash particulate matter derived from biofuel and diesel: implications for the reactivity of soot, J. Nanopart. Res. 14 (2012) 1224–1241.
[25] A. Liati, D.P. Eggenschwiler, M.E. Gubler, D. Schreiber, M. Aguirre, Investigation of diesel ash particulate matter: a scanning electron microscope and transmission electron microscope study, Atmos. Environ. 49 (2012) 391–402.
[26] F.E. Löpez Suárez, A. Bueno-López, M.J. Illán-Gómez, B. Ura, J. Trawczynski, Study of the uncatalyzed and catalyzed combustion of diesel and biodiesel soot, Catal. Today 176 (2011) 182–186.
[27] R. Jiménez, X. García, C. Cellier, P. Ruiz, A.L. Gordon, Soot combustion with K/MgO as catalyst, Appl. Catal. A 297 (2006) 125–134.
[28] R. Jiménez, X. García, C. Cellier, P. Ruiz, A.L. Gordon, Soot combustion with K/MgO as catalyst: II. Effect of K-precursor, Appl. Catal. A 314 (2006) 81–88.
[29] M.S. Gross, M.A. Ulla, C.A. Querini, Catalytic oxidation of diesel soot: new characterization and kinetic evidence related to the reaction mechanism on K/CeO$_2$ catalyst, Appl. Catal. A 360 (2009) 81–88.
[30] E. Aneggi, C. de Leitenburg, G. Dolcetti, A. Trovarelli, Diesel soot combustion activity of ceria promoted with alkali metals, Catal. Today 136 (2008) 3–10.
[31] R. Matarrese, L. Castoldi, L. Lietti, P. Forzatti, Soot combustion: reactivity of alkaline and alkaline earth metal oxides in full contact with soot, Catal. Today 136 (2008) 11–17.
[32] L. Castoldi, R. Matarrese, L. Lietti, P. Forzatti, Intrinsic reactivity of alkaline and alkaline earth metal oxide catalysts for oxidation of soot, Appl. Catal. B 90 (2009) 278–285.
[33] M.E. Gálvez, S. Ascaso, R. Moliner, M.J. Lázaro, Me (Cu, Co, V)-K/Al$_2$O$_3$ supported catalysts for the simultaneous removal of soot and nitrogen oxides from diesel exhausts, Chem. Eng. Sci. 87 (2013) 75–90.
[34] M.J. Valero-Romero, F.J. García-Mateos, J. Rodríguez-Mirasol, T. Cordero, Role of surface phosphorus complexes on the oxidation of porous carbons, Fuel Process. Technol. 157 (2017) 116–126.
[35] X. Wu, L.R. Radovic, Inhibition of catalytic oxidation of carbon/carbon composites by phosphorus, Carbon 44 (2006) 141–151.
[36] X. Wu, L.R. Radovic, Catalytic oxidation of carbon/carbon composite materials in the presence of potassium and calcium acetates, Carbon 43 (2005) 333–344.
[37] J. Schobing, V. Tschamber, A. Brillard, G. Leyssens, Impact of biodiesel impurities on carbon oxidation in passive regeneration conditions: influence of the alkali metals, Appl. Catal. B 226 (2018) 596–607.
[38] S. Liu, X.D. Wu, D. Weng, M. Li, J. Fan, Sulfation of Pt/Al$_2$O$_3$ catalyst for soot oxidation: high utilization of NO$_2$ and oxidation of surface oxygenated complexes, Appl. Catal. B 138-139 (2013) 199–211.
[39] Y. Wei, Z. Zhao, B. Jin, X. Yu, J. Jiao, K. Li, et al., Synthesis of AuPt alloy nanoparticles supported on 3D ordered macroporous oxide with enhanced catalytic performance for soot combustion, Catal. Today 251 (2015) 103–113.
[40] G.C. Dhal, S. Dey, D. Mohan, R. Prasad, Study of Fe, Co, and Mn-based perovskite-type catalysts for the simultaneous control of soot and NO$_x$ from diesel engine exhaust, Mater. Discovery 10 (2017) 37–42.
[41] A. Mishra, R. Prasad, Preparation and application of perovskite catalysts for diesel soot emissions control: an overview, Catal. Rev. 56 (2014) 57–81.
[42] B. Cui, S. Yan, Y.K. Xia, K. Li, S.R. Li, D. Wang, Y.Y. Ye, Y.Q. Liu, Cu$_x$Ce$_{1-x}$O$_2$ nanoflakes with improved catalytic activity and thermal stability for diesel soot combustion, Appl. Catal. A 578 (2019) 20–29.
[43] P. Sudarsanam, B. Hillary, M.H. Amin, N. Rockstroh, U. Bentrup, A. Bruckner, S.K. Bhargava, Heterostructured copper-ceria and iron-ceria nanorods: role of morphology, redox, and acid properties in catalytic diesel soot combustion, Langmuir 34 (2018) 2663–2673.
[44] F. Lin, X.D. Wu, S. Liu, D. Weng, Y.Y. Huang, Preparation of MnO$_x$-CeO$_x$-Al$_2$O$_3$ mixed oxides for NO$_x$-assisted soot oxidation: activity, structure and thermal stability, Chem. Eng. J. 226 (2013) 105–112.
[45] X.D. Wu, F. Lin, H.B. Xu, D. Weng, Effects of absorbed and gaseous NO$_x$ species on catalytic oxidation of diesel soot with MnO$_x$-CeO$_2$ mixed oxides, Appl. Catal. B 96 (2010) 101–109.
[46] H.L. Zhang, S.D. Yuan, J.L. Wang, M.C. Gong, Y.Q. Chen, Effects of contact model and NO$_x$ on soot oxidation activity over Pt/MnO$_x$-CeO$_2$ and the reaction mechanisms, Chem. Eng. J. 327 (2017) 1066–1076.
[47] S. Liu, X.D. Wu, D. Weng, M. Li, H.R. Lee, Combined promoting effects of platinum and MnO$_x$-CeO$_2$ supported on alumina on NO$_x$-assisted soot oxidation: thermal stability and sulfur resistance, Chem. Eng. J. 203 (2012) 25–35.
[48] I. Atribak, F.E. López-Suárez, A. Bueno-López, A. García-García, New insights into the performance of ceria-zirconia mixed oxides as soot combustion catalysts. Identification of the role of “active oxygen” production, Catal. Today 176 (2011) 404–408.
[49] A. Sadezky, H. Muckenhuber, H. Grothe, R. Niessner, U. Pöschl, Raman microspectroscopy of soot and related carbonaceous materials: spectral analysis and structural information, Carbon 43 (2005) 1731–1742.
[50] M. Knauer, M.E. Schuster, D.S. Su, R. Schlögl, R. Niessner, N.P. Ivleva, Soot structure and reactivity analysis by Raman microspectroscopy, temperature-programmed oxidation and high-resolution transmission electron microscopy, J. Phys. Chem. A 113 (2009) 13871–13880.
[51] Y. Wang, D.C. Alsmeyer, R.L. McCreery, Raman spectroscopy of carbon materials: structural basis of observed spectra, Chem. Mater. 2 (1990) 557–563.
[52] A. Cuesta, P. Dhamelincourt, J. Laureyns, A. Martinez-Alonso, J.M.D. Tascon, Raman microprobe studies on carbon materials, Carbon 32 (1994) 1523–1532.
[53] S.K. Sze, N. Siddique, J.J. Sloan, R. Escribano, Raman spectroscopic characterisation of carbonaceous aerosol, Atmos. Environ. 35 (2001) 561–568.
[54] T. Jawhari, A. Roid, J. Casado, Raman spectroscopic characterisation of some commercially available carbon black materials, Carbon 33 (1995) 1561–1565.
[55] B. Dippel, H. Jander, J. Heintzenberg, NIR FT Raman spectroscopic study of flame soot, Phys. Chem. Phys. 1 (1999) 4707–4712.
[56] K. Nakamura, M. Fujitsuka, M. Kitajima, Disorder-induced line broadening in first-order Raman scattering from graphite, Phys. Rev. B Condens. Matter 41 (1990) 12260–12263.
[57] M. Lapuerta, F. Oliva, J.R. Agudelo, A.L. Boehman, Effect of fuel on the soot nanostructure and consequences on loading and regeneration of diesel particulate filter, Combust. Flame 159 (2012) 844–853.
[58] C.D. Wagner, A.V. Naumkin, A. Kraut-Vass, J.W. Allison, C.J. Powell, J.R.J. Rumble, NIST X-ray Photoelectron Spectroscopy (XPS) Database, Version 3.5, (2003).
[59] A.M. Puziy, O.I. Poddubnaya, R.P. Socha, J. Gurgul, M. Wisniewski, XPS and NMR studies of phosphoric acid activated carbons, Carbon 46 (2008) 2113–2123.
[60] X.Y. Wang, L. Ran, Y. Dai, Y.J. Lu, Q.G. Dai, Removal of Cl adsorbed on Mn-Ce-La solid solution catalysts during CVOC combustion, J. Colloid Interface Sci. 426 (2014) 324–332.
[61] H.L. Zhang, J.L. Wang, Y. Cao, Y.J. Wang, M.C. Gong, Y.Q. Chen, Effect of Y on improving the thermal stability of MnO$_x$-CeO$_2$ catalysts for diesel soot oxidation, Chinese. J. Catal. 36 (2015) 1333–1341.
[62] M.E. Gálvez, S. Ascaso, P. Stelmachowski, P. Legutko, A. Kotarba, R. Moliner, M.J. Lázaro, Influence of the surface potassium species in Fe-K/Al$_2$O$_3$ catalysts on the soot oxidation activity in the presence of NO$_x$, Appl. Catal. B 152-153 (2014) 88–98.
[63] H.L. Zhang, S.S. Li, Q.J. Lin, X. Feng, Y.Q. Chen, J.L. Wang, Study on hydrothermal deactivation of Pt/MnO$_x$-CeO$_2$ for NO$_x$-assisted soot oxidation: redox property, surface nitrates, and oxygen vacancies, Environ. Sci. Pollut. Res. 25 (2018) 16061–16070.